References

BERTAUT, E. F. (1952). *J. Phys. Radium*, **13**, 499–505.
BERTAUT, E. F. (1978). *J. Phys. Chem. Solids*, **39**, 97–102.
BHAGAVANTAM, S. (1966). *Crystal Symmetry and Physical Properties*, pp. 82–99. London & New York: Academic Press.
BUSING, W. R. & LEVY, H. A. (1964). *Acta Cryst.* **17**, 142–146.
COCHRAN, W. (1954). *Acta Cryst.* **7**, 503–504.
COPPENS, P. (1975). *International Review of Science, Physical Chemistry Series Two*, **11**, 21–56. London: Butterworths.
HANSEN, N. K. & COPPENS, P. (1978). *Acta Cryst.* A**34**, 909–921.
HAREL, M. & HIRSHFELD, F. L. (1975). *Acta Cryst.* B**31**, 162–172.
HIRSHFELD, F. L. (1971). *Acta Cryst.* B**27**, 769–781.
HIRSHFELD, F. L. (1977*a*). *Isr. J. Chem.* **16**, 168–174.
HIRSHFELD, F. L. (1977*b*). *Isr. J. Chem.* **16**, 226–229.
HIRSHFELD, F. L. & RZOTKIEWICZ, S. (1974). *Mol. Phys.* **27**, 1319–1343.
International Tables for X-ray Crystallography (1974). Vol. IV. Birmingham: Kynoch Press.
NGO THONG & SCHWARZENBACH, D. (1979). *Acta Cryst* A**35**, 658–664.
STEWART, R. F. (1972). *J. Chem. Phys.* **57**, 1664–1668.
STEWART, R. F. (1973). *J. Chem. Phys.* **58**, 1668–1676.
STEWART, R. F. (1977). *Chem. Phys. Lett.* **49**, 281–284.

Acta Cryst. (1979). A**35**, 658–664

The Use of Electric Field Gradient Calculations in Charge Density Refinements. II. Charge Density Refinement of the Low-Quartz Structure of Aluminum Phosphate.

BY NGO THONG AND D. SCHWARZENBACH

Institut de Cristallographie, Université de Lausanne, Bâtiment des Sciences Physiques, 1015 *Lausanne, Switzerland*

(*Received* 19 *January* 1979; *accepted* 26 *February* 1979)

Abstract

The experimental determination of the electron distribution in quartz (SiO_2) is problematic since the structure is pronouncedly non-centrosymmetric. The structure of $AlPO_4$ is derived from the quartz structure by replacing half the Si atoms by Al and the other half by P. The physical properties of the two substances are similar. The electric field gradient tensor $\nabla\mathbf{E}$ at the site of Al (site symmetry 2) has already been measured. This electrostatic information, which is not available for quartz itself, is used in the determination of the charge density. Deformation parameters describing multipolar deformation functions are refined by least-squares methods with respect to X-ray data and the elements of the field gradient tensor simultaneously. A κ refinement yielded the atomic charges +1·4 for Al, +1·0 for P and −0·6 for O. The electron distribution obtained with a standard charge density refinement does not reproduce the correct $\nabla\mathbf{E}$. Inclusion of $\nabla\mathbf{E}$ in the refinement leads to a different least-squares minimum. The minimum is ill-defined by the X-ray data alone, whereas $\nabla\mathbf{E}$ stabilizes the phases of the superstructure reflections (l odd). $\nabla\mathbf{E}$ is extremely sensitive to the deformation density distribution. The resulting deformation maps show the maxima and minima always in the same places, but the inclusion of $\nabla\mathbf{E}$ changes the heights drastically and indicates the P—O bond to be more covalent than the Al—O bond. The trigonal arrangement of the lone-pair and bonding densities around the O atoms indicates sp^2 hybridization. This leads to bent covalent bonds, the angle Al—O—P being 142·3°. Double bonding appears to extend over nearly planar structural fragments defined by five atoms; metal—oxygen—metal—oxygen—metal.

Introduction

Several oxides with the composition $A^{III}B^{V}O_4$ form structures which can be derived from the isoelectronic SiO_2 modifications quartz, tridymite and cristoballite by replacing half the Si atoms by A and the other half by B. Buerger (1948) cites as examples BPO_4, $AlPO_4$, $FePO_4$, $GaPO_4$, $BAsO_4$ and $AlAsO_4$. The relationship between $AlPO_4$ and SiO_2 is particularly close. $AlPO_4$ forms all three structure types and shows the same polymorphic transformations at approximately the same temperatures as SiO_2. Large crystals of the low-quartz form of $AlPO_4$ (mineral name berlinite) were grown by hydrothermal synthesis (Stanley, 1954). Their physical properties are very similar to those of quartz (Schwarzenbach, 1966*a*); the density, hardness, refractive indices and optical rotatory power being all

0567-7394/79/040658-07$01.00

slightly smaller in $AlPO_4$. The main piezoelectric modulus d_{11} is $2{\cdot}3 \times 10^{-12}$ and $1{\cdot}4 \times 10^{-12}$ m.k.s. units for quartz and $AlPO_4$ respectively (Stanley, 1954). In addition, the $AlPO_4$ crystals were twinned according to the Brasilian and Dauphinée laws of quartz.

The crystal structure and absolute configuration of $AlPO_4$ determined from single-crystal X-ray diffraction with Cu $K\alpha$ and Mo $K\alpha$ radiation was published by Schwarzenbach (1966*a*). A difference synthesis in the centrosymmetric projection along [100] showed some residual electron density indicating the P—O bonds to be considerably more covalent than the Al—O bonds. The structure proved to be nearly identical to that of quartz even in such details as the size and orientation of the anisotropic temperature factor ellipsoids. The main difference between the two structures lies in the fact that the **c** axial length of $AlPO_4$ is twice that of quartz. In general, therefore, the reflections *hkl* with *l* even are stronger than those with *l* odd. The asymmetric unit contains one Al and one P atom on special positions with point symmetry 2, as well as two crystallographically independent but, with respect to bond lengths, identical O atoms in general positions. Whereas the space group $P3_221$ with a right-handed coordinate system is assigned to the right-handed dextrorotatory quartz structure [$I_o(10\bar{1}1) < I_o(10\bar{1}\bar{1})$, $z(+)$ corresponding to Donnay & Le Page, 1978], the analogous dextrorotatory $AlPO_4$ structure belongs to space group $P3_121$. This follows from purely geometrical considerations and is confirmed by the determination of the absolute configuration.

The electric field gradient tensor $\nabla\mathbf{E}$ at the site of Al in $AlPO_4$ has been measured by NQR spectroscopy (Brun, Hartmann, Laves & Schwarzenbach, 1961). Since Al possesses site symmetry 2, the tensor has three independent components. With the *x* and *z* axes of a local Cartesian coordinate system chosen along the twofold and threefold axes of the structure, these are ∇E_{11}, ∇E_{22}, $\nabla E_{33} = -(\nabla E_{11} + \nabla E_{22})$, ∇E_{23}, $\nabla E_{12} = \nabla E_{13} = 0$. The aim at that time was to compute $\nabla\mathbf{E}$ with a point charge model based on the accurate crystal structure in order to obtain information concerning O atom polarizabilities and the Sternheimer antishielding factor. The best fit with the experimentally determined tensor was obtained with dipole deformations of the O atoms which were oriented parallel to the bonding plane Al—O—P and inclined towards the P—O bond (Schwarzenbach, 1966*b*). This was qualitatively interpreted in terms of a more covalent P—O and a less covalent Al—O bond. The calculations also resolved the ambiguity of the sign of $\nabla\mathbf{E}$ which was experimentally not determined.

The first charge density analysis of quartz was carried out for a centrosymmetric projection by Brill, Hermann & Peters (1942). While their results, as well as the ones obtained for $AlPO_4$, undoubtedly show deviations from the spherical-atom model, the determination of three-dimensional charge density maps for this important basic structure is severely hampered by the fact that quartz is pronouncedly non-centrosymmetric. The use of a multipolar deformation model may permit us to obtain results with a least-squares refinement, but it is difficult to assess the uniqueness of such a solution. The $AlPO_4$ structure is sufficiently similar to that of quartz to be acceptable as a substitute, and it has the added advantage that the field gradient at the site of the Al nucleus is known. The presence of superstructure reflections *hkl* with *l* odd was considered to be advantageous since these are more strongly influenced by atomic asphericities. Their phases, however, tend to be less well-defined by the spherical-atom model (procrystal). We have therefore developed and applied a procedure (Schwarzenbach & Ngo Thong, 1979) which permits us to derive charge densities with a least-squares refinement of deformation parameters (Hirshfeld, 1977), the observations being X-ray intensities and field gradient tensor components.

Experimental

A batch of untwinned crystal fragments cut from a large specimen grown by Stanley (1954) had been prepared by Schwarzenbach (1966*a*). A plate 2 mm thick was cut perpendicular to **c** and etched in an aqueous solution of NH_4HF_2. A domain was accepted as untwinned if it showed only one orientation of the triangular etch figures on both sides of the plate which were moreover related by a twofold axis whose direction was established from morphology. One such fragment remained in the possession of the authors. Its optical activity indicated a dextrorotatory crystal

Table 1. *Crystal data and data collection*

Formula	$AlPO_4$
a (Å)	4·9423 (3)
c	10·9446 (13)
V (Å^3)	231·52 (4)
Z	3
F_{000}	180
Space group	$P3_121$
3 Al in (*a*)	$x0\frac{1}{3}$
3 P in (*b*)	$x0\frac{5}{6}$
6 O(1), 6 O(2) in (*c*)	xyz
No. of parameters	28
Radiation	Mo $K\alpha$, Nb-filtered $\lambda = 0{\cdot}70926$ Å
Scan method	2θ–θ
Background	minimal $\sigma(I)/I$
$\sin\theta/\lambda$ max (Å^{-1})	1·19
Data collected	$h + k \geq 0$, $h \geq 0$, $\pm l$
No. of reflections measured	5375
No. of unique reflections	1264
No. of reflections, $I < 3\sigma$	116
R of equivalent intensities	0·015
μ(Mo $K\alpha$) (mm^{-1})	1·004

(space group $P3_121$ as discussed above). It was ground to a sphere of diameter 0·283 mm with a crystal grinder (Nonius), and mounted on a Syntex $P2_1$ Fortran diffractometer. The lattice constants determined from a set of high-angle reflections were in excellent agreement with those measured earlier. Crystal data and important data collection parameters are shown in Table 1.

Four sets of equivalent reflections were measured with Mo $K\alpha$ radiation to a maximum $\sin\theta/\lambda$ of 1·19 Å^{-1}. In particular, the Friedel pair $\bar{h}\bar{k}\bar{l}$ was measured for every reflection *hkl*. The scattering power of the crystal was amply sufficient to extend data collection to higher angles. We felt, however, that this might introduce new uncertainties since dispersion corrections at high angles are not known and the TDS correction as well as anharmonic vibrations increases in importance. The intensity background was determined in time-sharing with data collection with an algorithm minimizing $\sigma(I)/I$ (Blessing, Coppens & Becker, 1972) modified by Schwarzenbach (1977) which permits a monitoring of doubtful reflection profiles. As in the earlier work (Schwarzenbach, 1966*a*), multiple diffraction effects were detected at the space-group extinctions 002 and 004. Extinction effects for some low-order reflections were again severe. Equivalent reflections were then averaged. The average of two intensities of a Friedel pair is $|F_{hkl}|^2 + |F_{\bar{h}\bar{k}\bar{l}}|^2 = |F'|^2 + |F''|^2$ where F' is computed with the real parts of the scattering factors and F'' with the imaginary parts. The latter are 0·095 for P, 0·052 for Al and 0·006 for O (*International Tables for X-ray Crystallography*, 1974). Model calculations show $|F''|^2$ to be negligibly small with respect to $|F'|^2$ for all reflections, and even more so if the scale factor is adjusted. The averaging of the Friedel pairs thus eliminates the imaginary part of the dispersion correction. The intensities of six periodically measured check reflections remained constant. The e.s.d.'s of the intensities were computed from counting statistics and the fluctuations of the check reflections about their mean, according to $\sigma^2 = \sigma^2$(statistics) + KI^2, $K = 0{\cdot}0002$. The e.s.d.'s of the structure factors were derived with the law of propagation of errors modified for small intensities (French & Wilson, 1978). This ensures that structure refinements with respect to $|F|$ and $|F|^2$ with weights $\sigma^{-2}(F)$ and $\sigma^{-2}(F^2)$ respectively lead to virtually the same results and goodness of fit. The absorption correction was negligible.*

Table 2. *Refined parameters and reliability factors*

The temperature factor expression used is $\exp[-2\pi^2\sum h_i h_j a_i^* a_j^* U_{ij}]$. The goodness of fit (GOF) is defined by $\sum$ weight × $(|F_o| - |F_c|)^2/(n - m)$ where n is the number of observations and m the number of variable parameters. α is the exponent of the radial charge deformation functions.

Parameter		Spherical-atom model (*a*)	κ refinement (*b*)	Charge density without ∇E (*c*)	Charge density with ∇E (*d*)
Al	*x*	0·46643 (5)	0·46646 (5)	0·46651 (7)	0·46650 (2)
	U_{11}	0·00754 (7)	0·00744 (6)	0·00767 (7)	0·00772 (3)
	U_{22}	0·00586 (7)	0·00576 (8)	0·00603 (9)	0·00603 (4)
	U_{33}	0·00633 (7)	0·00620 (6)	0·00647 (7)	0·00644 (3)
	U_{13}	−0·00015 (4)	−0·00016 (3)	−0·00012 (3)	−0·00012 (1)
	α			5·7 (3)	5·3 (3)
P	*x*	0·46685 (4)	0·46689 (4)	0·46690 (5)	0·46690 (2)
	U_{11}	0·00775 (6)	0·00761 (4)	0·00791 (6)	0·00792 (2)
	U_{22}	0·00544 (7)	0·00531 (6)	0·00564 (7)	0·00562 (3)
	U_{33}	0·00627 (6)	0·00612 (5)	0·00637 (6)	0·00636 (2)
	U_{13}	−0·00015 (3)	−0·00016 (2)	−0·00019 (2)	−0·00018 (1)
	α			5·8 (3)	5·7 (3)
O(1)	*x*	0·4163 (1)	0·4165 (1)	0·4160 (1)	0·41608 (3)
	y	0·2922 (1)	0·2921 (1)	0·2922 (1)	0·29224 (4)
	z	0·39770 (4)	0·39769 (3)	0·39759 (3)	0·39759 (1)
	U_{11}	0·0179 (2)	0·0177 (2)	0·0185 (2)	0·01850 (9)
	U_{22}	0·0123 (2)	0·0122 (1)	0·0127 (1)	0·01270 (7)
	U_{33}	0·0117 (1)	0·0116 (1)	0·0120 (1)	0·01200 (6)
	U_{12}	0·0100 (2)	0·0099 (1)	0·0105 (1)	0·01049 (8)
	U_{13}	−0·0031 (1)	−0·0031 (1)	−0·00315 (9)	−0·00318 (7)
	U_{23}	−0·0049 (1)	−0·0049 (1)	−0·00499 (7)	−0·00504 (5)
	α			4·7 (2)	3·8 (2)
O(2)	*x*	0·4156 (1)	0·4157 (1)	0·4153 (1)	0·41534 (4)
	y	0·2576 (1)	0·2577 (1)	0·2579 (1)	0·25791 (1)
	z	0·88365 (4)	0·88367 (4)	0·88353 (4)	0·88353 (2)
	U_{11}	0·0175 (2)	0·0173 (2)	0·0180 (2)	0·0180 (1)
	U_{22}	0·0117 (2)	0·0115 (1)	0·0119 (1)	0·01193 (7)
	U_{33}	0·0129 (1)	0·0128 (1)	0·0133 (1)	0·01332 (6)
	U_{12}	0·0101 (2)	0·0100 (1)	0·0105 (1)	0·01048 (7)
	U_{13}	−0·0042 (1)	−0·0043 (1)	−0·0044 (1)	−0·00441 (6)
	U_{23}	−0·0053 (1)	−0·0053 (1)	−0·0055 (1)	−0·00552 (5)
	α			4·7 (3)	4·1 (2)
Scale		1·000 (1)	0·995 (1)	1·024 (7)	1·0242 (4)
$R(F)$		0·022 (0·019*)	0·0177*	0·0165	0·0162
$R_w(F^2)$		0·044 (0·023*)	0·0183*	0·0181	0·0177
GOF		13·59 (3·72*)	3·22*	2·850	2·484†
Al–O(1)		1·7323 (6) Å	1·7314 (6)	1·7329 (6)	1·7328 (2)
Al–O(2)		1·7397 (4)	1·7392 (4)	1·7394 (5)	1·7395 (2)
P–O(2)		1·5201 (6)	1·5205 (6)	1·5220 (6)	1·5220 (2)
P–O(1)		1·5223 (4)	1·5226 (4)	1·5231 (4)	1·5229 (3)

* Observed reflections alone, $I > 3\sigma(I)$.
† Defined with respect to the X-ray data alone.

Structure and charge density refinements

Structural parameters and charge densities were obtained with five different refinements. The results and reliability indices are shown in Table 2. A projection of the structure is shown in Fig. 1.

(*a*) *Standard spherical-atom refinement*

The structure was first anisotropically refined with the program *CRYLSQ* of the *X-Ray System* (1972) to $R = 0{\cdot}019$. The scattering factors in analytical form and the real dispersion corrections were taken from *International Tables for X-ray Crystallography* (1974).

* Lists of structure factors and atomic parameters have been deposited with the British Library Lending Division as Supplementary Publication No. SUP 34308 (8 pp.). Copies may be obtained through The Executive Secretary, International Union of Crystallography, 5 Abbey Square, Chester CH1 2HU, England.

The isotropic extinction correction (Zachariasen, 1967) proved to be very important. The correction, y, according to $F_o = yF_{corr}$ for the strongest reflection, $10\bar{1}\bar{2}$, is equal to 0·741, *i.e.* 45% of the intensity is lost by extinction. Other large y values are 0·850 for $10\bar{1}2$, 0·886 for $20\bar{2}0$, and 0·900 for $10\bar{1}0$. 11 reflection intensities were affected by 10% or more. A supplementary refinement with the algorithm of Becker & Coppens (1975) executed at the University of Geneva surprisingly led to no improvement in R and goodness of fit. The previously obtained extinction correction was therefore used in all subsequent refinements.

Twinning of the crystal according to the Dauphinée law [001] would introduce severe errors into the structure factors since reflections hkl and $\bar{h}\bar{k}l$ from different twin domains would then superimpose. Although the crystal was selected in a way to make this effect unlikely, the program was modified to permit the refinement of a twin parameter K according to $|F_o|^2 = y^2[(1-K)|F_{hkl}|^2 + K|F_{\bar{h}\bar{k}l}|^2]$, y being the extinction factor. K was determined to be 0·00046 (12). R and the goodness of fit remained unchanged. Only the single-domain intensity of the weak reflection $30\bar{3}2$ would be noticeably affected by this parameter. Twinning was therefore presumed to be absent.

(*b*) *κ refinement and atomic charges*

Atomic charges were derived with the κ refinement (Coppens, 1977; Hansen & Coppens, 1978). The scattering factor of a spherical atom is assumed to be $f(S) = P_{core}f_{core}(S) + P_{valence}f_{valence}(S/\kappa)$, $S = \sin\theta/\lambda$. The population factor P_{core} is kept at the closed shell value. The valence population factor $P_{valence}$ and the parameter κ describing the expansion or contraction of the valence shell are refined. The free-atom core and valence scattering factors were taken from Fukamachi (1971). The program *CRYLSQ* was modified to permit the easy derivation of standard atomic charges in a variety of compounds. Any type of linear constraint is treated rigorously.

According to this refinement, the atomic charges are +1·4 (1) for Al, +1·0 (1) for P and −0·60 (4) for O, the corresponding κ factors are 1·09 (4), 1·03 (1) and 0·975 (4) respectively. Most gratifyingly, the results for the two O atoms, which were refined independently, differ by only 0·2 e.s.d.'s, indicating complete chemical equivalence. These charges confirm again the high covalency of the P—O bond.

(*c*) *Charge density refinement, X-ray data alone*

Extinction corrected data were transferred to the program *LSEXP* (Hirshfeld, 1977), modified according to Schwarzenbach & Ngo Thong (1979). The same scattering factors were used as in (*a*). All functions from $n = 0$ to 4, *i.e.* monopoles, dipoles, quadrupoles, octopoles and hexadecapoles were introduced without any non-crystallographic constraints, resulting in 108 population parameters and four exponents α of the radial functions $r^n\exp(-\alpha r)$. The 28 standard structural parameters and the scale factor were also varied. The electric-field-gradient tensor elements were not introduced as observations. The refinement converged readily. The quantity $\sum$ weight × $(|F_o|^2 - |F_c|^2)^2$ was examined as a function of sin θ/λ and $|F|^2$ and showed no significant trends. The rigid-bond test criterion (Hirshfeld, 1976), stating that for two atoms covalently bonded to each other the mean square amplitudes of vibration should be similar, was obeyed within twice the e.s.d.'s. The scale factor defined by $F_c \simeq$ scale × F_o increased by 2% and all the temperature factors increased correspondingly. The two P—O lengths became more similar whereas the difference between the two Al—O lengths remained unchanged.

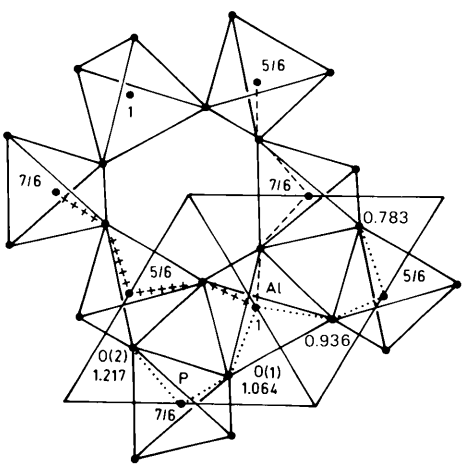

Fig. 1. Projection of the $AlPO_4$ structure showing the orientations of three least-squares planes metal—oxygen—metal—oxygen—metal. The dotted line includes also the P—O(2) bond which is inclined to the plane. Each plane contains a twofold axis.

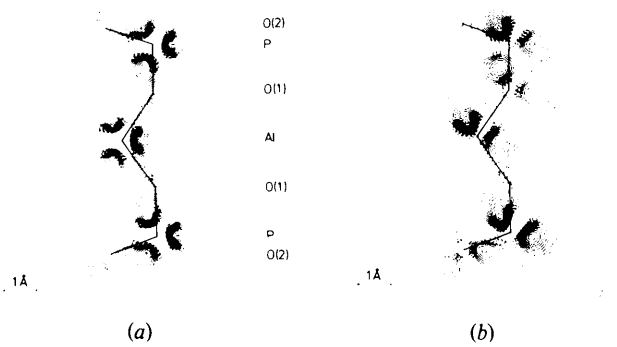

(*a*) (*b*)

Fig. 2. Deformation maps obtained from X-ray data alone (refinement *c*) in sections parallel to the plane P—O(1)—Al—O(1)—P. Negative contours broken, contour interval 0·1 e Å^{-3}. (*a*) Density in the plane; (*b*) density at height 0·3 Å.

The resulting deformation maps are shown in Figs. 2 and 3. They were computed with *DEFSYN* (Hirshfeld, 1977) and a locally developed plot program. The density was plotted in sections parallel to the least-squares planes defined by P–O(1)–Al–O(1)–P and Al–O(2)–P–O(2)–Al (Fig. 1). These are the most planar fragments of the structure, the O atoms deviating by about 0·5 Å from the plane. They contain the twofold axes which pass through the central metal atoms. The four tetrahedral bonds of a metal atom can thus be classified as two central bonds and two terminal bonds with respect to the planar fragments which show all the relevant features of the structure. Al and P show qualitatively similar deformation densities with respect to the distribution as well as similar heights of the bonding maxima. High densities appear near the bonds which all seem to be bent. The angles defined by the clearly visible O atom lone-pair density and the bonding maxima are approximately 120°. A high density maximum appears near the metal atoms in the acute angle of the central bonds with a corresponding negative region in the obtuse angle, *i.e.* the acute angle between the terminal bonds. The other maxima are cross sections through other bonds formed by the terminal metal atoms. The field gradient computed from these deformation maps (Table 3) does not agree at all with the experimental values.

(*d*) *Charge density refinement with the field gradient tensor*

The observed field gradient tensor elements were then introduced as observations in the refinement. The deformation density is thus modelled in such a way as to reproduce (in the least-squares sense) the diffraction data and the NQR results simultaneously. As shown by Schwarzenbach & Ngo Thong (1979), the field gradient due to the charge deformation alone has to be computed first, according to the relation

$$\nabla\mathbf{E}(\text{deformation}) = \nabla\mathbf{E}(\text{observed}) - \nabla\mathbf{E}(\text{overlap}),$$

$\nabla\mathbf{E}$(overlap) being the field gradient in the procrystal composed of spherical neutral atoms whose electron densities overlap at the site of Al. This quantity was evaluated considering the four nearest O atom neighbors at 1·74 Å and the four nearest P atom neighbors at 3·08 Å. The effect of the next nearest O atoms at 3·45 Å and longer distances and the next nearest metal atoms at 4·4 Å is negligibly small. Table 3 shows the overlap correction to be small and opposite in sign to the observed quantities. The observed tensor elements were assigned weights according to their e.s.d.'s. They were thus treated in the same way as the X-ray data.

It proved to be impossible to refine standard and deformation parameters at the same time. The refinement diverged, probably due to an increase of the correlations between positional, dipole and octopole parameters. The standard parameters were therefore fixed at their values of refinement (*c*) and the

Table 3. *Observed and calculated field gradient tensors at the site of* Al *in* $AlPO_4$ *in units* 10^{14} *e.s.u.*

Due to the site symmetry 2 of Al, $\nabla E_{12} = \nabla E_{13} = 0$. The Cartesian coordinate system is oriented with **x** parallel to the twofold and **z** parallel to the threefold axes.

	∇E_{11}	∇E_{22}	∇E_{33}	∇E_{23}
Observed	−3·790 (4)	2·395 (4)	1·395	0·48 (1)
Spherical-atom model (overlap)	0·065	−0·033	−0·032	−0·023
Observed minus overlap (deformation)	−3·855	2·428	1·427	0·503
Calculated from refinement (*c*)	−0·4129	1·5296	−1·1173	−4·1100
Calculated from refinement (*d*)	−3·8530	2·4273	1·4252	0·5040
Contribution of the electrons of the central Al, refinement (*d*)	−2·4999	4·7362	−2·2363	0·6041
Calculated from refinement (*e*)	−1·3445	1·2750	0·0692	−4·2124

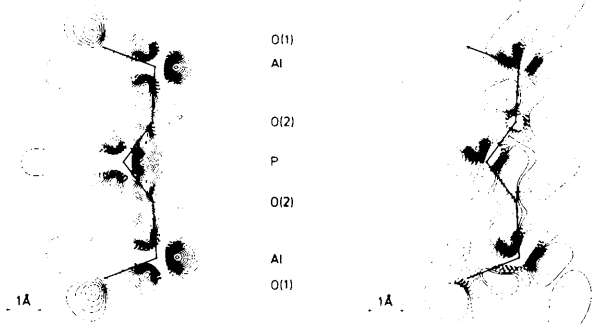

(*a*) (*b*)

Fig. 3. Deformation maps as in Fig. 2 for the plane Al–O(2)–P–O(2)–Al.

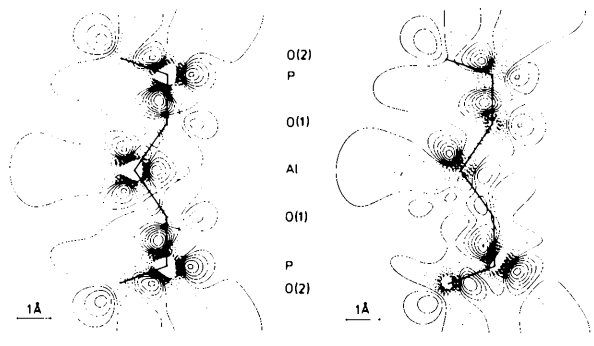

(*a*) (*b*)

Fig. 4. Deformation maps obtained with the field gradient (refinement *d*) in sections parallel to the plane P–O(1)–Al–O(1)–P. (*a*) Density in the plane; (*b*) density at height 0·3 Å.

deformation parameters alone were varied. After large initial shifts, the refinement converged to a goodness of fit of 2·682 ($R = 0{\cdot}0163$, $R_w = 0{\cdot}0178$) which is lower than the value obtained for refinement (*c*). The deformation parameters were then kept fixed and the standard parameters were refined. The shifts were all minimal, but the e.s.d.'s decreased considerably and the goodness of fit was lowered to 2·484. The observed and calculated field gradients are shown in Table 3. The contribution of the central atom Al alone computed with its even deformation functions is about 60% of the total field gradient. The temperature factor correction assuming independent vibrations of the atoms (Schwarzenbach & Ngo Thong, 1979) proved to be negligible.

The corresponding deformation maps are shown in Figs. 4 and 5, the e.s.d.'s in Fig. 6. They show all the maxima and minima of refinement (*c*) in the same places. The heights are, however, considerably different and generally lower. The central bonds now show clearly higher densities for P–O than for Al–O, and the maxima between them are strongly reduced.

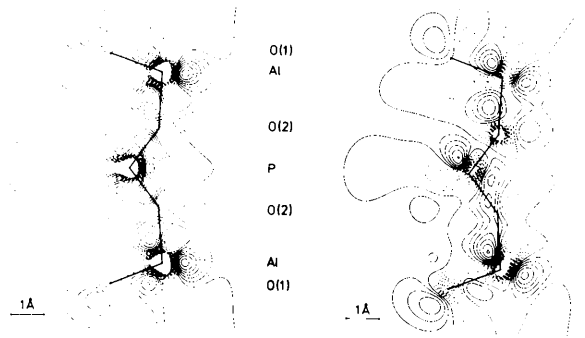

(*a*) (*b*)

Fig. 5. Deformation maps as in Fig. 4 for the plane Al–O(2)–P–O(2)–Al.

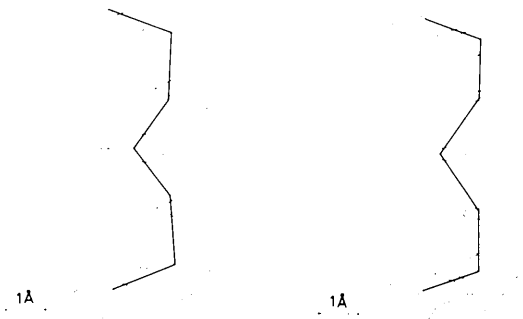

(*a*) (*b*)

Fig. 6. Error maps showing the e.s.d.'s obtained with refinement (*d*). Lowest contour 0·05 e Å^{-3}, contour interval 0·05 e Å^{-3}. (*a*) Plane P–O(1)–Al–O(1)–P; (*b*) plane Al–O(2)–P–O(2)–Al.

(*e*) *Charge density refinement, X-ray data alone, starting from refinement* (*d*)

The lowering of the reliability indices upon the introduction of the additional electrostatic information indicates that in fact a least-squares minimum has been reached which is different to the one attained with refinement (*c*). This is due to the behaviour of the superstructure reflections with *l* odd which define the difference between Al and P atoms. Had they all been omitted from the refinement, the two planes P–O(1)–Al–O(1)–P and Al–O(2)–P–O(2)–Al would have been identical as they are in the SiO_2 quartz structure. The positions of the maxima and minima are primarily determined by the main reflections with *l* even whose phases are adequately defined by the spherical-atom model and the centrosymmetric projections. An additional refinement was therefore computed starting with the parameters of the new minimum obtained in (*d*). This did not revert to the minimum of refinement (*c*). The reliability indices were hardly changed. The difference between the resulting maps and those of refinement (*d*) was small. All bond maxima decreased by about 1 e.s.d., but the difference between the heights of the Al–O and the P–O bond peaks remained unchanged. Only the maximum between the central bonds of Al increased. The O atom lone-pair densities were also not altered. The field gradient computed from this refinement is again in bad agreement with the observations, showing its great sensitivity to the electron distribution. It seems to be considerably influenced by the maximum between the central bonds of Al. The least-squares minimum with respect to the X-ray data alone is very shallow and ill-defined.

Discussion

The electron density maps obtained for $AlPO_4$ show very considerable electron transfers with respect to the free-atom model. The minima at the O atom positions indicate an expansion of the valence density distribution of these atoms. The two crystallographically independent O atoms are very similar, the *central* P–O bonds being more covalent than the *central* Al–O bonds. The *terminal* bonds differ less and show higher densities. The two bonding planes, which would be identical in the quartz structure, are otherwise completely analogous. All covalent bonds are bent. The bond maxima for the *terminal* bonds lie in the bonding plane metal–oxygen–metal–oxygen–metal, but displaced from the lines connecting the nuclei. The metal atoms participate in two terminal bonds, *viz* Al–O(2) and P–O(1). They are thus situated in the middle of one and at the limits of two other bonding planes (Fig. 1). The bond maxima of the central bonds are displaced perpendicular to the bonding plane defined by them, but

they are not far from the two other planes terminating at the metal atom, as evidenced by the electron distributions around the terminal metal atoms in Figs. 4 and 5. They are connected by an electron bridge culminating in a considerable maximum near the metal. The charge density around the metal is thus very asymmetric and shaped like a bag whose opening is indicated by the minimum between the two terminal bonds. Central bonds are all slightly shorter than terminal bonds, 1·733 and 1·522 Å for Al–O(1) and P–O(2), and 1·739 and 1·523 Å for Al–O(2) and P–O(1) respectively.

The lone-pair densities of the O atoms are also displaced by about 0·3 Å from the bonding plane. The angles subtended at the O atom by the bond maxima and these lone-pair densities are roughly 120°. Oxygen appears thus to be sp^2 hybridized. The angle defined by the nuclear positions is, however, 142·3°. The density distribution appears thus to favor a 120° angle which can, however, not be attained since it would imply non-bonded O–O distances considerably shorter than the observed distances starting at 3·45 Å. The triangular O atom seems to be placed into the structure in such a way as to move the bond maxima as near to the internuclear vectors as possible. The electron bridge extending over both central bonds indicates p_π–d_π bonding within the plane and could be obtained by an overlap of the two O atom p_z orbitals with a metal d_{xz} orbital (x along the twofold axis, z perpendicular to the plane). The terminal metal atoms possess one central bond lying approximately in the plane defined by these p_z orbitals. The orientations of their d orbitals, defined with respect to their proper bonding planes, are all oblique to the direction of p_z(oxygen), indicating that the resonance might extend only over the bonding plane. The difference between terminal and central bonds is clearly shown by the higher localized density maxima of the former, as opposed to the diffuse electron bridge over the latter.

Concluding remarks

Our results show that charge densities in this non-centrosymmetric structure can indeed be obtained. The refinements with respect to the X-ray data alone and our new procedure lead to solutions with similar reliability indices for the structure factors. Moreover, the maps have the positions of the maxima in common. The electric-field-gradient tensor, on the other hand, is very sensitive to the deformation density, so that it remains doubtful whether it can ever be computed from X-ray data alone. Alternatively, $\nabla\mathbf{E}$ need not be known very accurately to be successfully used in our procedure. Its introduction in the refinement modifies mainly the phases of the superstructure reflections. We believe the resulting charge density maps of Figs. 4 and 5 to be superior to those of Figs. 2 and 3 since they show much smaller maxima between the central bonds and more analogous electron distributions around Al and P. They also indicate more ionic Al–O bonds and more covalent P–O bonds. We repeat, however, our earlier remark that the maps are not observed, but constructed in such a way as to reproduce the results of two types of experiments by assuming that the X-ray intensities and the electric field gradient are functions of the same set of parameters. In a later paper, we will describe the charge density distribution in quartz based on X-ray data. It is entirely consistent with that obtained for $AlPO_4$, and shows again the maximum between the central bonds.

We thank Dr H. D. Flack, University of Geneva, for his help in evaluating extinction corrections. The calculations were carried out at the Computer Center, Swiss Federal Institute of Technology at Lausanne (CDC CYBER NOS/BE). This project is supported by the Swiss National Science Foundation, grant no. 2.724-0.77.

References

BECKER, P. J. & COPPENS, P. (1975). *Acta Cryst.* A**31**, 417–425.

BLESSING, R. H., COPPENS, P. & BECKER, P. J. (1972). *J. Appl. Cryst.* **7**, 488–492.

BRILL, R., HERMANN, C. & PETERS, CL. (1942). *Ann. Phys. (Paris)*, **41**, 233–244.

BRUN, E., HARTMANN, P., LAVES, F. & SCHWARZENBACH, D. (1961). *Helv. Phys. Acta*, **34**, 388–391.

BUERGER, M. J. (1948). *Am. Mineral.* **33**, 751.

COPPENS, P. (1977). *Isr. J. Chem.* **16**, 159–162.

DONNAY, J. D. H. & LE PAGE, Y. (1978). *Acta Cryst.* A**34**, 584–594.

FRENCH, S. & WILSON, K. (1978). *Acta Cryst.* A**34**, 517–525.

FUKAMACHI, T. (1971). *Mean X-ray Scattering Factors Calculated from Analytical Roothan–Hartree–Fock Wave Functions by Clementi.* Tech. Rep. Ser. B, no. 12, Institute for Solid State Physics, Univ. of Tokyo.

HANSEN, N. K. & COPPENS, P. (1978). *Acta Cryst.* A**34**, 909–921.

HIRSHFELD, F. L. (1976). *Acta Cryst.* A**32**, 239–244.

HIRSHFELD, F. L. (1977). *Isr. J. Chem.* **16**, 226–229.

International Tables for X-ray Crystallography (1974). Vol. IV. Birmingham: Kynoch Press.

SCHWARZENBACH, D. (1966*a*). *Z. Kristallogr.* **123**, 161–185.

SCHWARZENBACH, D. (1966*b*). *Z. Kristallogr.* **123**, 422–442.

SCHWARZENBACH, D. (1977). *Collect. Abstr. Fourth Eur. Crystallogr. Meet.* PI.20.

SCHWARZENBACH, D. & NGO THONG (1979). *Acta Cryst.* A**35**, 652–658.

STANLEY, J. M. (1954). *Ind. Eng. Chem.* **46**, 1684–1689.

X-Ray System (1972). Techn. Rep. TR-192. Computer Science Center, Univ. of Maryland, College Park, Maryland. Implemented and extended by D. SCHWARZENBACH.

ZACHARIASEN, W. H. (1967). *Acta Cryst.* **23**, 558–564.